Electronic Supplementary Material (ESI) for Analyst.

Supplementary information

Rapid isolation of Cf-DNA from large-volume whole blood on centrifugal microfluidic chip based on immiscible phase filtration

Fei Hu, Juan Li, Niancai Peng*, Zheng Li, Zengming Zhang, Shuhao Zhao, Mingyue Duan , Hui Tian, Lei Li, Peng Zhang

The supporting material includes:

a. Theoretical derivation of interface stability of immiscible phases during the rotating state - Supplemental Figures S1 and S2

b. The specific volume of the chambers in the disk - Supplemental Table S1

c. Rotational frequency protocol - Supplemental Table S2

d. Reagent dosage - Supplemental Table S3

e. Performance steps for whole blood and plasma - Supplemental Table S4

f. Positive standard amplification - Supplemental Figure S3 and Table S5

g. Hemolytic test - Supplemental Figure S4

h. Other studies using IFAST method to isolate nucleic acids - Supplemental Table S6

i. Comparison of magnetic bead recovery between manual and disk methods - Supplemental Table S7

j. The experiment of the device reproducibility - Supplemental Figure S5

k. Comparison with other nucleic acids isolation and detection methods

l. The certification to prove that our lab was approved by the local IRB - Supplemental Figure S6

Theoretical derivation of interface stability of immiscible phases during the rotating state

When the fluid rotates at different angular velocities and angular accelerations in the chamber, both the pressure throughout the liquid and the fluid pressure in the microchannel will change. The key for the microchannel design is to preserve the shape of the liquid distribution at the microchannel position during the rotation. If the angular velocity or the angular acceleration of the rotation are too large, the pressure difference between both sides of the microchannel interface may exceed the adaptability of the surface tension. Then, the flow path will be disrupted, thus causing fluid mixing in adjacent chambers. Therefore, it is necessary to analyze the distribution law of the fluid pressure in the chamber during rotation.

Considering the shape of the channel, a cylindrical coordinate system is used for the analysis. The height direction is the z direction, the bottom surface of the channel is the z = 0 plane, the intersection of the channel axis and the z = 0 plane is the origin, and the other two directions are r and θ. Since the propagation velocity of the pressure in the liquid far exceeded the linear velocity of the rotation, it can be assumed that at any time point during the rotation process, the fluid in the chamber reached equilibrium, i.e., a quasi-equilibrium state, in which the pressure distribution obeys the following rules:

$$\begin{cases} -\dfrac{\partial p}{\partial r} - \rho g_r = \rho a_r \\ -\dfrac{1}{r}\dfrac{\partial p}{\partial \theta} - \rho g_\theta = \rho a_\theta \\ -\dfrac{\partial p}{\partial z} - \rho g_z = \rho a_z \end{cases} \quad (1)$$

Where, p represents the static pressure of the fluid particle, ρ represents the fluid density, g represents the acceleration of gravity, and a represents the acceleration of the fluid micro-element. $g_r = 0$, $g_\theta = 0$, g_z=g; $a_r = -r\omega^2$, $a_\theta = \beta r^2$, $a_z = 0$, ω, where represents the angular velocity and β represents the angular acceleration.

The above equation yields:

$$\frac{\partial p}{\partial r}=\rho r\omega^2 \quad \frac{\partial p}{\partial \theta}=-\rho\beta r^2 \quad \frac{\partial p}{\partial z}=-\rho g \qquad (2)$$

The differential equations with r, θ, and z as independent variables can be expressed as:

$$dp=\frac{\partial p}{\partial r}dr+\frac{\partial p}{\partial \theta}d\theta+\frac{\partial p}{\partial z}dz \qquad (3)$$

Substituting (2) into (3) yields:

$$dp=\rho r\omega^2 dr-\rho\beta r^2 d\theta-\rho g dz \qquad (4)$$

For the stable liquid surface during the rotation, the pressure is equal at any point, i.e.: $dp=0$. Then, the differential equation for the stable liquid surface can be obtained:

$$\rho r\omega^2 dr-\rho\beta r^2 d\theta-\rho g dz=0 \quad (5)$$

Integrating the differential equation (5) along dr=0 (the direction of the same radius, i.e. the circumferential direction) yields:

$$-\beta r^2 d\theta-g dz=0 \quad (6)$$

It can be obtained that:

$$z=-\frac{\beta}{g}r^2\theta+C_1 \qquad (7)$$

Integrating equation (6) along $d\theta$=0 (the direction of the same angle, i.e. the radial direction) yields:

$$r\omega^2 dr-g dz=0 \qquad (8)$$

It can be obtained that:

$$z=\frac{\omega^2}{2g}r^2+C_2 \qquad (9)$$

Combining (7) and (9) yields:

$$z=\frac{\omega^2}{2g}r^2-\frac{\beta}{g}r^2\theta+C \qquad (10)$$

The above equation is a geometric expression of the free liquid surface, where C is an unknown number, that needs to be obtained according to the conservation condition,

which is a function of the angular velocity ω and the angular acceleration β, i.e., C = C(ω, β).

Assuming that the air pressure is p_a, the pressure at the left side of the chamber connected to the microchannel is p_l, the pressure at the right side connected to the microchannel is p_r, and thus, according to Equation (4), the following relationship exists:

$$p_l = p_a + \rho\left(gC + \frac{1}{2} r_1^2 \omega^2 \right) \tag{11}$$

$$p_r = p_a + \rho\left(gC + \frac{1}{2} r_1^2 \omega^2 - \beta r_1^2 (\theta_2 - \theta_1) \right) \tag{12}$$

If the other side of the microchannel is connected to air, i.e., if the pressure on the other side is p_a, then, the pressure differences of the two-phase interfaces of the microchannel are:

$$\Delta p_l = \rho\left(gC + \frac{1}{2} r_1^2 \omega^2 \right) \tag{13}$$

$$\Delta p_r = \rho\left(gC + \frac{1}{2} r_1^2 \omega^2 - \beta r_1^2 (\theta_2 - \theta_1) \right) \tag{14}$$

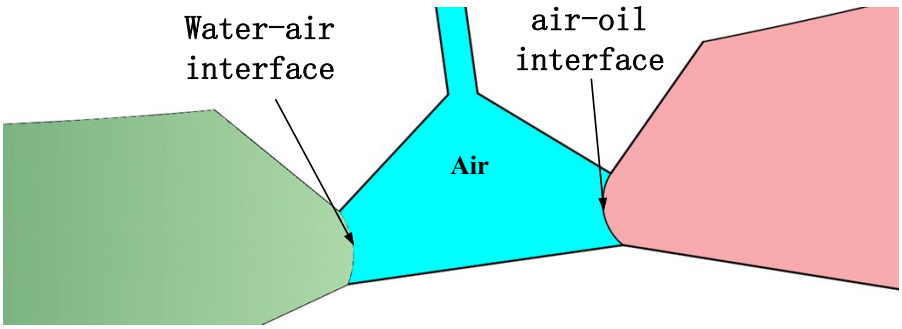

Fig. S1. Interface diagram

The two-phase liquid forms a liquid surface as shown in Fig. S1 at the microchannel position. If the liquid surface remains stable, the shape of the liquid surface conforms to the Laplace equation:

$$\Delta p = \frac{\sigma}{R} \qquad (15)$$

During the rotation process, if p_w increases, R decreases (i.e., the liquid surface curvature increases), d also decreases, and the liquid advances toward the air side. When the liquid advances to the minimum position of the microchannel, while p_w still increases, then, the liquid will cross both the air chamber and the microchannel and flow to the other chamber. At this time point, the artificially disposed virtual wall can be considered to be in a state of "breakdown". Consequently, the water phase and the oil phase mix, and the separation device will fail to work normally. The state in which p_w enables the formation of the liquid surface at the narrowest position is a critical state, during which the allowable maximum value Δp_{max} of Δp is determined by the fluid property and the flow path structure. During the rotation, if p_w decreases, then R and d increase, and the liquid advances toward the liquid chamber side. In this case, there is no risk of mixing multiple liquids.

When $\Delta p_{max} \leq \Delta p_l$ ($\Delta p_{max} \leq \Delta p_r$), the interface can remain stable; however, when $\Delta p_{max} > \Delta p_l$ ($\Delta p_{max} > \Delta p_r$), the interface cannot remain stable and the microchannel will be "punctured".

During the actual chip design process, an arch bridge microchannel was designed. The position of the water-air interface and the oil-air interface is at the near core end with respect to the chamber position. To improve the adaptability of the interfacial tension, the surface of the air chamber is treated with fluorosilane to both reduce the surface energy and increase the interfacial tension between air and water/oil.

To further verify that there is a reasonable combination of acceleration and angular acceleration to maintain the stability of the immiscible phase interface from the analytical solution, the Δp contour map is drawn using Matlab software, as shown in Fig. S2. Fig. S2 not only reflects the state in which the angular velocity ω is in the same direction than the acceleration β, but also reflects the state in which the angular velocity ω and the angular acceleration β are in reversed directions. Figure S2 shows that during the start-up rotation process of the chip (ω = 0, β = 0), the interface of the immiscible phase bears a large pressure difference, and consequently, it starts up with a small

acceleration. When the rotational angular velocity exceeds a critical state line, the immiscible phase fluid returns to the respective chambers and there is no liquid in the microchannel. Due to the rotation of the disk and the acceleration and deceleration, the chamber liquid near the end of the microchannel is "cleaved". Consequently, it retracts toward the far-end of the chamber. In this state, the liquid between the air microchamber and the liquid chamber is blocked, and air can flow freely. Therefore, it can be accelerated to the target speed at any acceleration to meet specific experimental requirements.

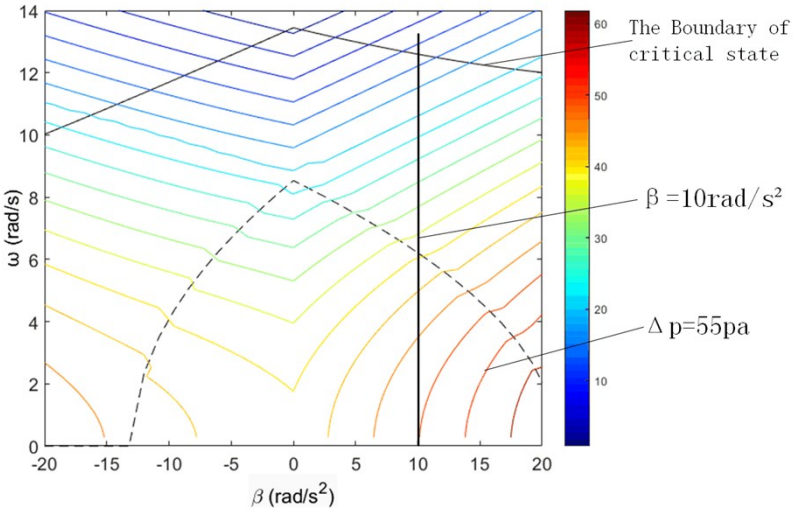

Fig. S2 Pressure contour under different ω-β states

Here, it is assumed that Δp = 55 Pa, which is determined by the fluid properties and structure. As shown in Figure 2, the Δp = 55 Pa contour is identified. Before reaching the critical state line at an acceleration of 10 rad/s^2, the Δp = 55 Pa contour will not be intersected. After reaching the target speed, any acceleration can be used to reach the target speed. In the actual experiment, to ensure that the immiscible phase fluid does not become miscible, the starting acceleration was set to 10 rpm/s (1.05 rad/s^2), and the critical rotation speed was set to 120 rpm (12.56 rad/s), which was experimentally verified.

Table S1. Specific volumes of the four chambers in the disk.

Chamber	Chamber volume (μl)
C1	4150
C2	3380
C3	544
C4	153

Explanation: C1-plasma separation chamber; C2-lysis/binding chamber; C3-imiscible phase chamber; C4-elution chamber

Table S2. Operation steps for the rapid isolation of Cell-free Nucleic Acids from large-volume whole blood

Step	Spin-speed (rpm)	Time s (s)	Operation
1	0-120(acceleration 10 rpm/s)	12	A small acceleration to guarantee each phase immiscible
2	3600(acceleration 500 rpm/s)	240	Plasma separation
3	350(deceleration 50 rpm/s)	30	Activation of the passive siphon
4	600(acceleration 20 rpm/s)	30	Transfer 1 ml plasma into sample chamber of cfDNA extraction,
5	120-840(acceleration 420 rpm/s and deceleration 180 rpm/s)	150	Mixing PMPs with plasma and lysis/binding buffer and promoting DNA bound to the PMPs
6	120-0(deceleration 10 rpm/s)	12	Slow deceleration to ensure a stable interface
7	0	120	Transferring PMPs across the air and oil barriers and into the elution buffer
8	0-120(acceleration 10 rpm/s)	12	The same as step 1
9	120-240(acceleration 420 rpm/s and deceleration 180 rpm/s)	150	Mixing PMPs in elution chamber. The DNA bound is released into the elution
10	120-0(deceleration 10 rpm/s)	12	The same as step 6

Table S3. Description of the reagents loaded in four chambers on the disk

Chamber	Reagents	Reagent volume (μl)
C1	Blood	4000
C2	Nucleic acid extraction reagent	silica-coated magnet beads suspended(15μl), lysis/binding buffer (1250 μl)
C3	Oil (silicone oil)	400
C4	Elution	50

Explanation: C1-plasma separation chamber; C2-lysis/binding chamber; C3-imiscible phase chamber; C4-elution chamber

Table S4. Performance steps required for C-IFAST extraction from whole blood and plasma

Process	Sample from whole blood	Sample from plasma
step	4a-4h	4d-4h

Different performance steps required for C-IFAST extraction, which was started from whole blood (Fig 4a-4h) and plasma (Fig 4d-4h)

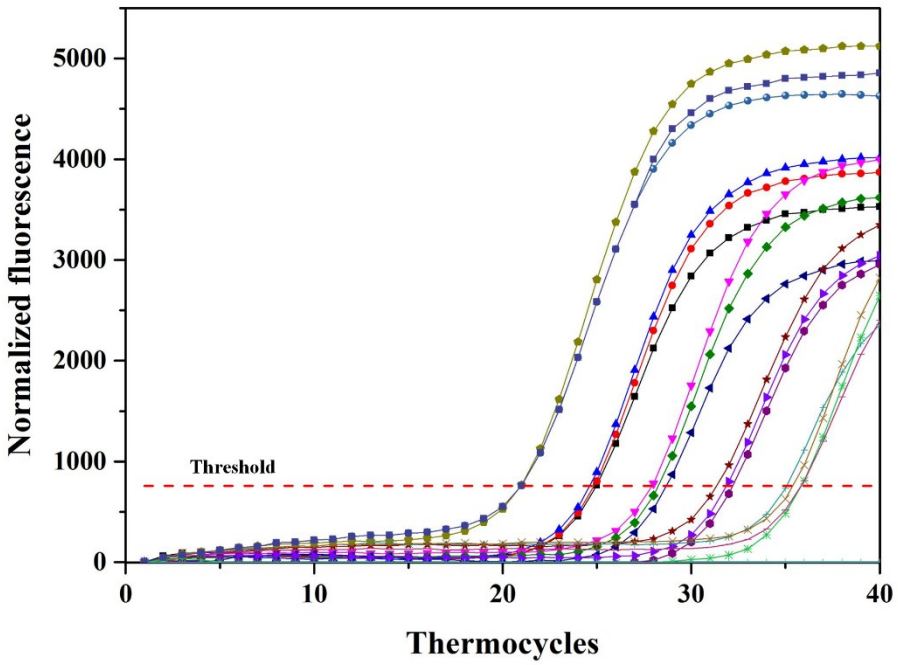

Fig. S3 Fluorescence PCR amplification curve. To verify the nucleic acid recovery rate of the chip, the positive standard was amplified in the Tianlong fluorescence quantitative kit and the amplified product was gradient diluted (100-200 bp) for the fluorescence PCR quantitative analysis. It was then used to mimic the cfDNA and verify the recovery rate of the chip. The conducted steps include: (1) amplification of the kit positive standard; (2) the amplification product was gradient diluted under outdoor conditions to prevent pollution, with dilutions ranging from 10^3 to 10^6 times. (3) Compound tube (three tubes) amplification of diluted sample PCR amplification was performed using the following protocol: 94 °C for 10 min followed by 40 cycles of 94 °C for 2 min, 55 °C for 2 min, and 72 °C for 2 min, with a final extension of 72 °C for 10 min, with 30 µl of final PCR volume: 1.5 µl each of a pair of primers (forward, reverse), 1.5 µl of probes, 10 µl of DI water, 3 µl dNTPs (2.5 mM), 2 µl reaction buffer (100 mM), 0.5 µl of Taq DNA polymerase and10 µl of template DNA.

Table S5. Different concentrations after amplification and dilution of HBV positive standard. Other concentrations are diluted according to the same method for the experimental requirements.

Sample	CT value	Concentration(copies/mL)
1	35.118	0.782×10^4
2	31.003	1.003×10^5
3	27.437	1.026×10^6
4	23.950	0.983×10^7
5	20.595	0.887×10^8

Hemolytic test

Whether hemolysis occurs during the process of plasma separation not only depends on the centrifugation speed but also on the centrifugation time. Therefore, the control of centrifugation speed and centrifugation time is central. A low centrifugation speed and short centrifugation time might lead to insufficient separation, while a high centrifugal speed and a long centrifugal time might cause hemolysis. To explore the effect of centrifugation conditions on plasma purity, the presented device was used to conduct hemolytic tests.

The whole blood was centrifuged on the presented disk and the supernatant plasma was collected in the sample chamber of DNA extraction after transfer via siphon valve. The results were observed under a microscope. Plasma was separated from whole blood by centrifugation at 3600 rpm initially and after 2 min, 3 min and 4 min (Fig. S4 a) of centrifugation. The pictures show that with increasing centrifugation time, fewer and fewer blood cells could be found in the plasma, and after centrifugation at 3600 rpm for 4 min, more than 95% of the blood cells were removed. However, this phenomenon does not indicate that the longer the time, the better the results. When the centrifugation time reaches a threshold, blood cells could rupture and cause hemolysis, which negatively affects plasma purity.

The hemolysis of blood cells can be characterized via the content of heme. If red blood cells break, the hemoglobin in the cells will escape into the solution. The hemoglobin has the maximum absorbance at 414 nm. By measuring the absorbance at 414 nm, the amount of heme in the sample could be characterized and thus, it could be clarified whether hemolysis had occurred. The higher the absorbance of the supernatant obtained after centrifugation at 414 nm, the higher the content of free heme, and a more severe hemolysis of red blood cells was caused by the separation process.

To determine the optimal centrifugation speed and centrifugation time, different centrifugation speeds (3000 rpm, 3600rpm, and 4000 rpm) and different centrifugal times (3 min, 4 min, 5 min, 6 min, and 7 min) were used for each speed. UV-visible spectrophotometer (U-2800, HITACHI, Japan) was used to measure the absorption at 414 nm. First, the initial blood sample was diluted five times with deionized water to

completely dissolve the red blood cells due to the low osmotic pressure, release hemoglobin, and obtain a positive control sample. Then, the initial blood sample was centrifuged at 1500 r/min for 5 min by centrifuge (H1850, Cence, China). The supernatant was collected and cleaned to obtain a blank control sample. Next, whole blood samples were added to the plasma separation chamber of the presented disk. Then, the disk was subjected to the tested centrifugation speeds and centrifugation times to obtain the plasma supernatant for these various conditions. At last, the absorbance values of all supernatants were measured using UV-visible spectrophotometer. The experiment showed that the whole blood was centrifuged at 3000 rpm for 3-7 min, the absorption values were far lower than that of the positive control and similar to that of the blank control (Fig. S4 c). Therefore, the sample was not affected by hemolysis. When the whole blood was centrifuged at 3600 rpm, during the first 5 min (3 min, 4 min, and 5 min), no hemolysis was found. However, when for centrifugation time of 6 min and 7 min, the absorbance values clearly increased compared to the blank control (Fig. S4 b). This indicates slight hemolysis. Similarly, when 4000 rpm was applied to the whole blood, within the 6 min and 7 min, slight hemolysis was found (Fig. S4 d). Considering all these factors, 3600 rpm and 4 min, were identified as optimal centrifugation speed and centrifugation time, respectively.

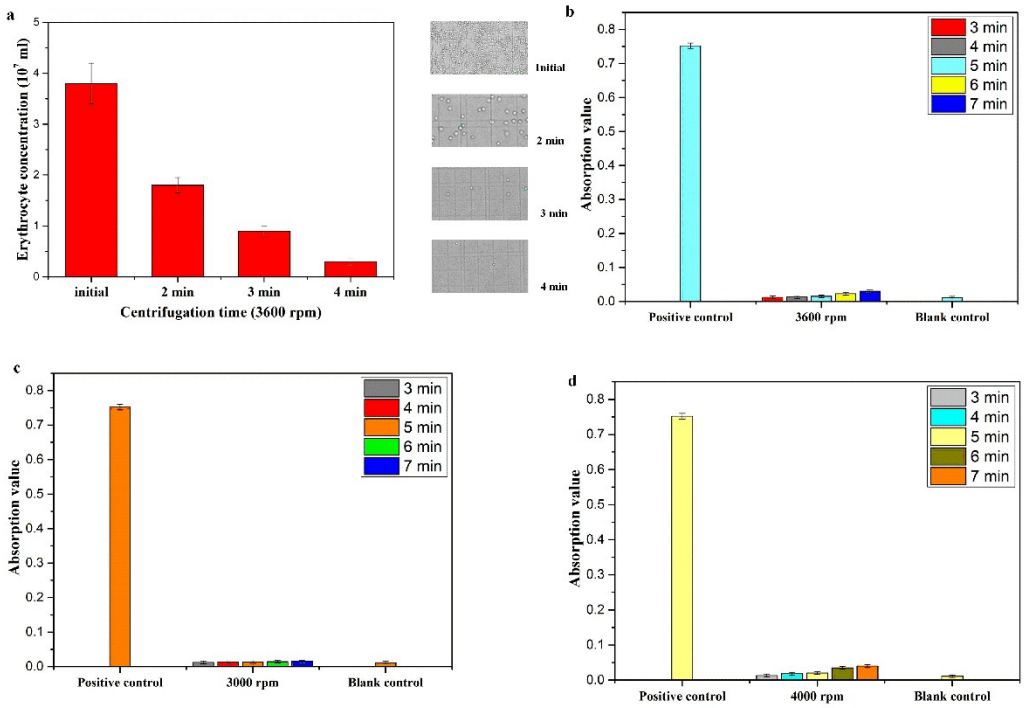

Fig. S4 Optimal centrifugation speed and centrifugation time for plasma separation. (a) Comparison of red blood content between initial sample and separated products which for different centrifugation times (2 min, 3 min, and 4 min). (b) Comparison of the absorption values among positive control, blank control, and products at 3600 rpm (c) at 3000 rpm (d) at 4000 rpm, centrifuged for different centrifugation times (3 min, 4 min, 5 min, 6 min, and 7 min).

Table S6 Other studies using IFAST method to isolate nucleic acids

Study	Immiscible phase	Target	Recovery
Dulk et al.[32]	Paraffin wax	Plasmid DNA from plasma samples	35-70%
Mosley et al.[21]	Mineral oil	Helicobacter pylori	About 55%
Bordelon et al.[34]	Air	Syncytial virus (RSV) RNA	55%(spike TE buffer) and 33%(lysates of RSV infected HEp-2 cells)
Lei Zhang et al.[35]	Castor oil	HPV plasmid	61%
This study	Silicone oil	Spiked HBV (mimic cfDNA)	65% from plasma and 30% from whole blood

Table S7 Weight of dry bead pellets before and after transfer by manual and disk method, respectively.

Dry magnetic beads pellets	Initial weights (mg)	Weights recovered by manual method (mg)	Recovery rate (%)
1	1.85	1.78	96.2
2	2.03	1.98	97.5
3	1.98	1.89	95.4
4	2.01	1.87	93
5	1.87	1.77	94.7
6	2.08	1.95	93.8
Average Recovery			95.1±1.49

Dry magnetic beads pellets	Initial weights (mg)	Weights recovered by disk method (mg)	Recovery rate (%)
1	1.83	1.57	85.8
2	1.95	1.71	87.8
3	1.89	1.54	81.5
4	2.04	1.70	83.3
5	1.97	1.69	85.8
6	2.12	1.81	85.4
Average Recovery			84.9±2.0

The experiment of the device reproducibility

The presented chip is single-use for fear of contamination. Therefore, device-to-device experiments were conducted to test the reproducibility of the results generated with different chips. One chip has two identical structures which can analyze two samples at the same time. The chip was used to detect HBV with two different concentrations (10^3 copies/ml and 10^4 copies/ml) to mimic the 100-200 bp cfDNA. Experiments were started from the whole blood sample and plasma sample, respectively, and were conducted 30 times each. The time series extraction results for different samples (whole blood and plasma) are shown in Fig. S5. Experiments showed, that the average number of template DNA for 10^3 copies/ml was 663 copies/ml with a coefficient of variation (CV) of 7.25% (n = 30) and 6520.8 copies/ml with a coefficient of variation (CV) of 4.48% (n = 30) for 10^4 copies/ml from the plasma sample. The template DNA for 10^3 copies/ml was 306 copies/ml with a coefficient of variation (CV) of 9.14% (n = 30) and 3152 copies/ml with a coefficient of variation (CV) of 5.21% (n = 30) for 10^4 copies/ml from whole blood sample.

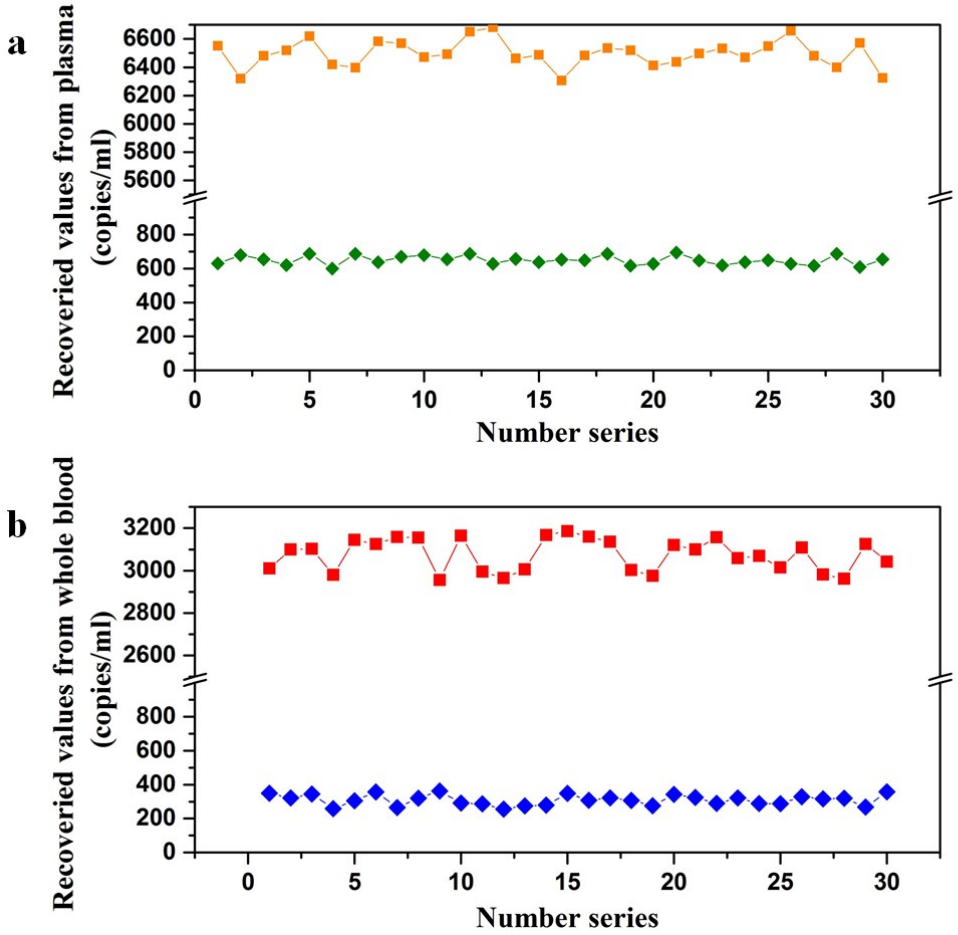

Fig. S5 DNA extraction results for 30 repetitions of each concentration and each sample (10^3 copies/ml and 10^4 copies/ml; whole blood sample and plasma sample) to test the reproducibility of the chip. (a) Statistical illustration of the plasma DNA extraction results. (b) Statistical illustration of the whole blood DNA extraction results.

Table S8 Comparison with other nucleic acids isolation and detection methods. (NR=Not reported)

Study	Target	Method	Sample	Total time	Detection in chip
Jeon et al.[12]	cfDNA	Ppy-coated Au nanowires to capture and release cfDNA	Plasma(200 μL)	>35 min	No
Omiccioli et al.[13]	cfDNA	Magnetic capture hybridization technology	Plasma	NR	No
Sonnenberg et al.[16]	cfDNA	Dielectrophoresis (DEP)	Blood(25 μl)	10 min	No
Shiddiky et al.[14,15]	miRNA	magnetic beads-coupled capture probe sequences	Cell	>30 min	Yes
Kim et al.[27]	cfDNA	Traditional magnetic beads method	Blood(3 ml)	<30 min	No
This study	cfDNA	C-IFAST method	Blood(4 ml)	<15 min	No

Affiliated Children's Hospital of Xi'an Jiaotong University

Medical Ethics Committee

Ethical Approval Document

Ref. No.: 2018-079
Received date: 23/10/2018

Project Title:	Study on the Separation and Extraction of Cell Free Nucleic Acids of Human Peripheral Blood		
Data Collection Period: ☑ **From** 01/03/2018 **to** 31/03/2019 **(dd/mm/yyyy).** ☐ **Not applicable as no new data will be collected.**			
Funding Source: ☑ Foundation ☐ Goverment ☐ Corporation ☐ International organization ☐ Others **Gran No:** National Natural Science Foundation of China (No: 61827827)			
Principal Investigator:	Peng Niancai	**Title:**	Professor
Department:	School of Mechanical Engineering, Xi'an Jiaotong University		
Tel:	18091883695	**Email:**	ncpeng@mail.xjtu.edu.cn
Student Investigator:	Hu Fei	**Student no.:**	4113001107

Co-Investigators	**Department /institution**	**Position**	**Programme**	**Email**

Review Determinations of Medical Ethics Committee

☑ **Approval** ☐ **Disapproval** ☐ **To revise**

Professor Peng Niancai's research project Separation and Extraction of Human Peripheral Blood Free Nucleic Acids utilize peripheral blood samples for free nucleic acid isolation and extraction. Peripheral blood samples are from laboratory healthy volunteers and Affiliated Children's Hospital of Xi'an Jiaotong University will assist in the collection of blood samples. After review of Application Form, Confidentiality Agreement, Consent Form and other related documents, this project conforms to medical ethical principles and is approved by Ethical Medical Ethics Committee.

Signature of Medical Ethics Committee Director: 李安茂印

Signature of Medical Ethics Committee: 医学伦理委员会

Fig. S6 The certificate to prove that ethics approval was obtained from the Institutional Human Research Ethics Committee of the Affiliated Children's Hospital of Xi'an Jiaotong University (Approval No. 2018-079)